coatings

IMPACT FACTOR 3.4

CITESCORE 4.7

Article

High-Aligned PVDF Nanofibers with a High Electroactive Phase Prepared by Systematically Optimizing the Solution Property and Process Parameters of Electrospinning

Zhongchen He, François Rault, Astha Vishwakarma, Elham Mohsenzadeh and Fabien Salaün

Special Issue
Functional Polymer Films and Their Applications

Edited by
Prof. Dr. Galina K. Elyashevich

MDPI

https://doi.org/10.3390/coatings12091310

coatings

MDPI

Article

High-Aligned PVDF Nanofibers with a High Electroactive Phase Prepared by Systematically Optimizing the Solution Property and Process Parameters of Electrospinning

Zhongchen He [1], François Rault [1], Astha Vishwakarma [1], Elham Mohsenzadeh [1,2] and Fabien Salaün [1,*]

[1] ENSAIT, ULR 2461-GEMTEX-Génie et Matériaux Textiles, L'Université de Lille, F-59000 Lille, France
[2] Junia, F-59000 Lille, France
* Correspondence: fabien.salaun@ensait.fr

Abstract: Poly(vinylidene fluoride) (PVDF)-electrosprayed nanofibers have been the subject of much research due to their flexibility and piezoelectric properties compared to other piezoelectrics, for example, ceramics or other polymeric materials. The piezoelectric performance of PVDF is mainly related to the presence of β-phase. This study aims to determine the influence of working and formulation parameters on the generation of β-phase, morphology, and crystal structure of PVDF nanofibers. In addition, this research innovatively analyzes the effect of the dispersion state of PVDF molecular chains in the solvent on the electrospinning results. The morphology and crystal structure of PVDF nanofibers were determined using scanning electron microscopy (SEM), differential scanning calorimetry (DSC), and Fourier transform infrared spectroscopy (FTIR). Beadless nanofibers are obtained when the PVDF concentration reaches the semi-diluted regime entangled in dimethylformamide (DMF) or DMF/acetone solution. The optimization of the process parameters (static collector, tip to collector distance—25 cm, flow rate—1 mL/h, applied voltage—20 kV) allows the increase in the β-phase fraction from 68.3% ± 1.2% to 94.5% ± 0.6% for a PVDF concentration of 25 w/v% in a DMF/acetone mixture (2/3 v/v). With these same parameters applied to a rotating collector, it was observed that the piezoelectric performance is at maximum for a maximum β-phase fraction of 90.6% ± 1.1%, obtained for a rotational speed of 200 rpm. The effect of orientation of PVDF nanofibers on piezoelectric properties was quantitatively discussed for the first time; the piezoelectric properties are independent of the alignment of the nanofibers.

Keywords: PVDF nanofibers; electrospinning; electroactive phase; semidilute entangled; orientation

check for updates

Citation: He, Z.; Rault, F.; Vishwakarma, A.; Mohsenzadeh, E.; Salaün, F. High-Aligned PVDF Nanofibers with a High Electroactive Phase Prepared by Systematically Optimizing the Solution Property and Process Parameters of Electrospinning. *Coatings* **2022**, *12*, 1310. https://doi.org/10.3390/coatings12091310

Academic Editor: Günter Motz

Received: 22 July 2022
Accepted: 31 August 2022
Published: 7 September 2022

1. Introduction

Due to the increasingly severe energy shortage and environmental pollution problems, some new energy sources are receiving more research and attention. An example is the development of solar and wind farms that can generate several gigawatts per year [1]. In addition, energy harvesting devices based on the piezoelectric effect can also be selected as a new energy source [2]. The piezoelectric effect alters mechanical energy into electrical energy, and, as a result, piezoelectric materials find numerous applications in electromechanical fields [3]. The use of electronics in our daily lives is so widespread that a portable and wearable piezoelectric energy harvesting device could provide cleaner energy and make our daily lives more convenient. Traditional ceramic piezoelectric materials have excellent piezoelectric properties (for example, the piezoelectric coefficient of $PbZr_xTi_{1-x}O_3$ (PZT) is over than 300 pC/N [4], AlN is 3–5 pm/V, and ZnO is 14–26 pm/V [5]). Despite this, ceramic materials lack flexibility and high density, limiting their application fields and making it challenging to prepare wearable piezoelectric devices.

Besides ceramic materials, researchers have also found that some polymer materials such as poly(vinylidene fluoride) (PVDF) [6], poly(vinylidene fluoride-trifluoroethylene) (PVDF-TrFE) [7], polystyrene (PS) [8], polyacrylonitrile (PAN) [9], and poly(lactic) acid

(PLA) [10] possess specific piezoelectric properties, and can be used as piezoelectric materials. As well as their piezoelectric properties, these polymer materials have the advantages of easy processing, flexibility, low density, and high break strength. They are used in various piezoelectric applications and incredibly wearable piezoelectric applications [11–13]. PVDF ($(-CH_2-CF_2-)_n$) is a thermoplastic semi-crystalline polymer obtained from the free-radical polymerization of $CH_2=CF_2$. Due to its superior piezoelectric performance and lower price than other polymer materials, PVDF has been studied since 1969, when Kawai discovered the piezoelectric effect of PVDF films [14]. There are five different polymorphs in PVDF crystalline structure, named α-, β-, γ-, δ-, and ε-phases [15]. The nonpolar α phase is the standard form in PVDF, but it does not contribute to the piezoelectric properties of PVDF. The polar β- and γ-phases of PVDF exhibit excellent piezoelectric responses due to their high dipolar moment per unit cell (e.g., β phase 8×10^{-30} C·m [16]). As a result, the piezoelectric performance of PVDF is mainly determined by the content of polar crystalline phases (electroactive phase) [17]. The piezoelectric performance of PVDF can be further improved if the content of α in PVDF is reduced while the content of β and γ phases in PVDF is increased. PVDF is widely studied because of its potential piezoelectric properties in the field of energy harvesters [18], energy storage [19], sensors [20], actuators [21], batteries [22], and biomedical devices in the form of fibers or films [23].

The nanofiber structure can improve the piezoelectric potential of PVDF even further than the film structure. Ghosh et al. pointed out that deformation can be more effectively limited by axial direction if the size of the structures in the orthogonal direction is reduced [24]. If mechanical stress is applied along an axis, strain is generated in this axis direction and the orthogonal direction. If the size in the orthogonal direction (fiber diameter) is reduced, the strain is more effectively limited in the axis direction. The geometric limitation leads to a better alignment of the dipoles in piezoelectric materials, increasing the piezoelectric potential. According to Surmenev et al., the nano configuration promotes the orientation of the polymer chains and improves the piezoelectric response along the orientation direction of the molecular dipoles [25]. Thus, as a new type of material structure, nanofibers have attracted more and more attention in recent research. Although there are many other methods for producing nanofibers (centrifugal spinning [26], gas-assisted spinning [27], etc.), electrospinning is the most commonly used method to obtain PVDF nanofibers [28]. The electrospinning system consists of a syringe pump equipped with a needle (tip extrusion system), a voltage power supply, and an electrically conducting collector. The basic principle of electrospinning consists of the uniaxial stretching of a viscoelastic polymer solution in an electrical field. The electric field causes the polymer chain orientation and polarization [29]. The orientation and polarization of the polymer chain result in PVDF nanofibers with higher crystallinity and electroactive phase than PVDF nanofibers obtained by other methods [30]. In the research of Gee et al. [31], they discussed the influence of different solvents and voltages on the content of electroactive phases of PVDF. For example, adding acetone volatilizes the solvent entirely during electrospinning and increases the electroactive phase content. However, their research hardly mentioned the effect of solvent on electrospinning results from a microscopic scale (e.g., the dispersion state of PVDF molecular chains in solvent molecules). Wu et al. [32] prepared randomly oriented and aligned electrospun PVDF nanofibers. The results pointed out that the electroactive phase and piezoelectric property of aligned electrospun PVDF nanofibers is higher than of randomly oriented ones. However, in their research, the electrospinning parameters of randomly oriented and aligned electrospun PVDF nanofibers were different, and it was impossible to conclude that the improvement in piezoelectric property and electroactive phase is attributed to the aligned fiber distribution. Furthermore, they did not quantitatively differentiate "randomly oriented" and "aligned oriented".

This work analyzes the effects of various electrospinning parameters on the piezoelectric properties of PVDF nanofibers (e.g., solution and process parameters). The influences of the Coulomb forces provided by the electric field, the volatility of the solvent, and mechanical stretching on PVDF nanofibers were examined. In addition, this research analyzes the

effect of the PVDF concentration on the electrospinning results from the microscopic scale to find a correlation with the four different regimes (dilute, semidilute unentangled, semidilute entangled, and concentrated). The structures and properties of PVDF samples obtained by electrospinning are different when PVDF molecular chains are in different regimes, which has a guiding effect for the research of electrospinning/electrospray to obtain PVDF samples with different structures. At the same time, this study quantitatively discussed the impact of the orientation of PVDF nanofibers on piezoelectric properties for the first time, and the results showed that the piezoelectric properties of PVDF nanofibers were affected by the content of the electroactive phase rather than the orientation of PVDF nanofibers.

2. Materials and Methods

2.1. Materials

Poly(vinylidene fluoride) (PVDF) (Kynar@ 705) with a molecular weight of about 220,000 g·mol^{-1} was obtained from Arkema (Colombes, France) as the piezoelectric polymer. N, N-Dimethylformamide (DMF) and acetone, employed as PVDF solvents, were purchased from CARLO ERBA (Val-de-Reuil, France). All the selected compounds were used without further purification.

2.2. PVDF Nanofibers Electrospinning

2.2.1. Preparation of PVDF Solutions

A series of PVDF electrospinning solutions at different concentrations (5, 10, 15, 20, 25, and 30 w/v%) were prepared using DMF, and a mixture of DMF/acetone (2/3 v/v) was kept at 60 °C under vigorous magnetic stirring (800 rpm) equipped with a water-jacketed reflux condenser for 2 h. Before their usage, they were cooled to room temperature (25 °C).

2.2.2. Production of PVDF Nanofibers

A CAT000002 Electrospray Starter Kit from Spraybase® AVECATS (Kildare, Ireland) was used to carry out the electrospinning process for the different working solutions at room temperature with a static collector (metal plate with aluminum foil). The solutions were pumped with a digitally controlled syringe pump at a flow rate (FR) of 1 mL/h through a single stainless-steel nozzle (20 gauge, single nozzle, inner and outer diameters of 600 and 910 μm).

To analyze the influence of the solvent choice (DMF or DMF/acetone (2/3 v/v)) and PVDF concentration (PVDF = 5, 10, 15, 20, 25, and 30 w/v%) on the nanofiber morphology and electroactive phases, the working parameters were set at 20 kV for the applied voltage (V), 20 cm for the tip-to-collector distance (TCD), and 1 mL/h for the flow rate (FR). After setting the solution parameters, the effects of the apparatus parameters were determined by setting the applied voltage in the range between 15 to 30 kV (PVDF = 25 w/v% in DMF/acetone (2/3 v/v), TCD = 20 cm, and FR = 1 mL/h), the TCD value between 13 to 25 cm (PVDF = 25 w/v% in DMF/acetone (2/3 v/v), V = 20 kV, and FR = 1 mL/h), and the flow rate between 0.3 to 3 mL/h (PVDF = 25 w/v% in DMF/acetone (2/3 v/v), V = 20 kV, and TCD = 25 cm).

The previously set parameters (PVDF = 25 w/v% in DMF/acetone (2/3 v/v), V = 20 kV, TCD = 25 cm, (PVDF = 25 w/v% in DMF/acetone (2/3 v/v), V = 20 kV, and FR = 1 mL/h) and FR = 1 mL/h) were used to observe the influence of a rotating collector and its rotating speed with a Fluidnatek/LE-50 electrospinning apparatus (Bioinicia, Valencia, Spain). The rotating speed was set to 0, 200, 500, 1000, 1500, and 2000 rpm.

2.3. Analytical Methods

2.3.1. Solutions Viscosity

The viscosity of the solutions was measured by a rotational viscosimeter, Rheomat RM 100 (Lamy Rheology, Champagne-au-Mont-d'Or, France), with a shear rate ranging from 0.38 to 1420 s^{-1} at room temperature, corresponding to the range of shear rates at the top

of the tip. According to Higashi et al. studies, the shear force undergone by the solution during the electrospinning process can be approximated by Equation (1) [33].

$$\dot{\gamma} = \frac{4Q}{\pi R^3} \tag{1}$$

where $\dot{\gamma}$, Q and R are the shear rate at the needle wall (s^{-1}), the flow rate (mL/h), and the radius of the needle (mm), respectively. The estimated shear rate in the shear stress region was to be 14 s^{-1} for a flow rate value of about 1 mL/h, and with a 20-gauge needle.

2.3.2. Morphological Characterization of the Nanofibers

The morphology of the samples was characterized by scanning electron microscopy (SEM) (Phenom ProX, Thermo Fischer Scientific, Waltham, MA, USA). The samples were mounted on a metal holder and coated with gold using a sputter coater for 30 s followed by observation at an accelerating voltage of 5–15 kV. Image J software (National Institutes of Health, Bethesda, Rockville, MD, USA) was used to determine fiber mean diameter from SEM images from 100 random measurements.

2.3.3. Identification and Quantification of the Electroactive β and γ-Phases of the Poly(vinylidene fluoride) Nanofibers

Fourier transform infrared spectroscopy (FTIR) and differential scanning calorimetry (DSC) provide information on the presence of β, γ, and α phases. The use of both techniques was necessary because of the overlapping peaks, and a deconvolution method was used not only to make the correct phase identification but also to distinguish the different crystal forms.

- Differential scanning calorimetry

The crystallinity of the samples was characterized by Differential Scanning Calorimetry (DSC 6000, PerkinElmer, Boston, MA, USA). The sample space was purged with nitrogen flow during the experiments. Samples of 8–10 mg were placed in an aluminum pan and heated from 10 to 200 °C at 10 °C/min, and the sample was then cooled from 200 to 10 °C at a rate of 30 °C/min. The crystallinity index (X_c) of the sample was calculated according to Equation (2) [34].

$$X_c = \frac{\Delta H_m}{x_\alpha \Delta H_\alpha^0 + x_\beta \Delta H_\beta^0 + x_\gamma \Delta H_\gamma^0} \times 100\% \tag{2}$$

where ΔH_m is the specific melting enthalpy of the PVDF, and ΔH_α^0, ΔH_β^0, and ΔH_γ^0 are the theoretical specific melting heat of 100% crystalline enthalpies of α-, β-, and γ- crystalline PVDF phases of a 100% crystalline PVDF sample, which are taken as 103.4 J/g and 93.07 J/g for the α and β phases, respectively [35]. The specific melting heat of the γ phase is assumed to be identical to that of a 100% α phase [34].

The determination of the three peak areas was realized by the deconvolution of DSC curves between 150 to 180 °C using OriginPro 2019 (OriginLab Corporation, Northampton, MA, USA), with the package Peak Deconvolution (OriginLab Corporation, Northampton, MA, USA). Second derivative finding peak and Savitzky Golay's smooth derivative were used for the identification, and the Gaussian curve was selected to fit the deconvoluted curves.

- Fourier transform infrared spectroscopy

The identification of the crystal phases of the PVDF nanofiber samples was performed by Fourier transform infrared (FT-IR) spectra with a Nicolet Nexus (Nexus-560 spectroscopic, Nicolet, Madison, WI, USA) connected to a PC. FT-IR spectra were performed using attenuated total reflection (ATR) at a resolution of 4 cm^{-1}, across the spectral range of 4000–650 cm^{-1} and by the accumulation of 64 scans. To identify electroactive phases, the study area was restricted to 650–1600 cm^{-1} [36].

The relative fraction of the electroactive phase was calculated from Equation (3) [37].

$$F_{EA} = \frac{I_{EA}}{\frac{K_{840}}{K_{763}} I_{763} + I_{EA}} \times 100\% \quad (3)$$

where I_{EA} and I_{763} are the absorption values at 840 and 763 cm^{-1}; K_{763} (6.1×10^4 $cm^2 \cdot mol^{-1}$) and K_{840} (7.7×10^4 $cm^2 \cdot mol^{-1}$), respectively; and the absorption coefficients at the respective wavenumbers, respectively.

To provide an interpretation on a more quantitative basis and to determine the β and γ phase fractions, deconvolution of the spectra using OriginPro 2019 (OriginLab Corporation, Northampton, MA, USA), with the package Peak Deconvolution (OriginLab Corporation, Northampton, MA, USA), in the 920–700 cm^{-1} region into Gaussian peaks was realized. These wave numbers were initial parameters for curve fitting with Gaussian component peaks. Position, bandwidths, and amplitudes of the peaks were varied until (i) the resulting bands shifted by no more than 4 cm^{-1} from the initial parameters, (ii) all the peaks had reasonable half-widths (<20–25 cm^{-1}), and (iii) good agreement between the calculated sum of all components and the experimental spectra was achieved ($r^2 > 0.99$).

The fractions of the β and γ phases were calculated from Equations (4) and (5).

$$F(\beta) = F_{EA} \times \left(\frac{A_\beta}{A_\beta + A_\gamma} \right) \times 100\% \quad (4)$$

$$F(\gamma) = F_{EA} \times \left(\frac{A_\gamma}{A_\beta + A_\gamma} \right) \times 100\% \quad (5)$$

where A_β and A_γ are the areas of the β and γ peaks.

2.3.4. Piezoelectric Properties of the Poly(vinylidene fluoride) Nanofibers

The PVDF nanofibrous membranes' piezoelectric coefficient (d_{33}) was measured by a YE2730A piezoelectric d_{33} meter (Sinocera Piezotronics, Yangzhou, China). Frequency and stress were set to 110 Hz and 0.25 N, respectively. Each sample was in the size of 2×2 cm^2 and measured five times to obtain the average d_{33}.

2.3.5. Orientation of PVDF Nanofibers

- Anisotropy index

The orientation analysis of PVDF nanofibers was obtained using orientation matrix (Ω) and anisotropy index (α) (Equations (6) and (7)) [38].

$$\Omega = \frac{1}{I_{tot}} \sum I_i \begin{vmatrix} cos^2\theta_i & sin\theta_i\, cos\theta_i \\ sin\theta_i\, cos\theta_i & sin^2\theta_i \end{vmatrix} \quad (6)$$

$$\alpha = 1 - \lambda_1/\lambda_2 \quad (7)$$

where I_i (nm) is the length of the fiber, I_{tot} (nm) is the total sum of fiber lengths, and θ_i (°) is the angle between each fiber and the x-axis. I_i and θ_i were obtained from the SEM image analysis using Image J software, with 50 randomly selected nanofibers. λ_1 and λ_2 are the eigenvalues of the orientation matrix, with $\lambda_1 \leq \lambda_2$. The α is a factor describing the alignment scheme (α = 0: complete random distribution of nanofibers, α = 1: total aligned distribution of nanofibers).

- Goodness

From SEM image analyses with Image J, the goodness of fit of the Gaussian distribution, Goodness, was evaluated (Goodness = 0, random distribution of nanofibers; Goodness = 1, nanofibers are perfectly aligned in the same direction).

3. Results and Discussion

3.1. Influence of the Formulation Parameters on the Morphology of the PVDF Electropsun Mat

The fission and solidification processes of electrospun fibers are also closely related to the physical and chemical properties of the working solutions. Thus, there are relationships between the physicochemical properties of the solutions and the structure, morphology of electrospun PVDF nanofibers related to the choice of the solvents system, and the concentration of PVDF used. During electrospinning, the formation and shape of the Taylor cone, the break-up of charged polymer solution, and the solvent evaporation were governed by the physico-chemical properties of the solutions and the operating parameters.

The formation of electrospun fibers is closely related to the initial entanglement of PVDF macromolecular chains in solution. During solubilization, PVDF–PVDF interactions are transformed into PVDF–solvent interactions. The entanglement influences the morphology and average diameter of the resulting material during the electrospinning process, either fibers or beaded nanofibers. To ensure the formation of electrospun fibers, solvents with higher solubility for PVDF and higher volatility are not recommended [39].

A binary solvent system can also be used to dissolve PVDF to control the structure and morphology of the fibers and the solvent evaporation during the flying process. The degree of entanglement is related to the PVDF concentration used in the starting solution and, therefore, to the viscosity of the solutions. The dissolution state of the polymer in the solution is divided into four different regimes, (1) dilute, (2) unentangled semi-dilute, (3) entangled semi-dilute, and (4) concentrated [40]. The overlap concentration (C*) is the boundary between the dilute and the semi-dilute regimes. For this concentration, PVDF–solvent interactions begin to be replaced by polymer–polymer interactions. Nevertheless, most macromolecular chains are still not entangled. An increase in concentration leads to an increase in entanglement. The semi-unentangled to the semi-entangled regime corresponds to the entanglement concentration (C_e). According to Gupta et al., when the concentration is higher than C_e, electrospinning the solution results in uniform beadless fibers [41].

The viscosity of the solution increases with the increase in PVDF concentration (Figure 1). When the concentration of PVDF is 10 w/v%, the curve's slope changes. This shows that 10 w/v% is the C* of the PVDF/DMF system. When the concentration of PVDF/DMF exceeds 10 w/v%, as the concentration increases, the viscosity of the solution increases, and the slope does not change again. Furthermore, the morphology of the obtained structure changes with the increase in the solution concentration (Figure 2). Thus, flat and aggregated particles are obtained for concentrations lower than 10 w/v%. The average diameter of the particles increases along with their size distribution, until pearled fibers or microspheres linked together by fibers are obtained from 30 w/v%. In any case, it is impossible to obtain fibers under the conditions of the applied studies. Furthermore, when the PVDF concentration is more than 30 w/v%, electrospinning cannot be performed due to the high viscosity of the solution, inducing polymer deposition on the needle surface and jet instability. Therefore, the PVDF/DMF system is not conducive to obtaining electrospinning PVDF nanofibers without beads. It is necessary to find a way to reduce the solution's viscosity and the beads.

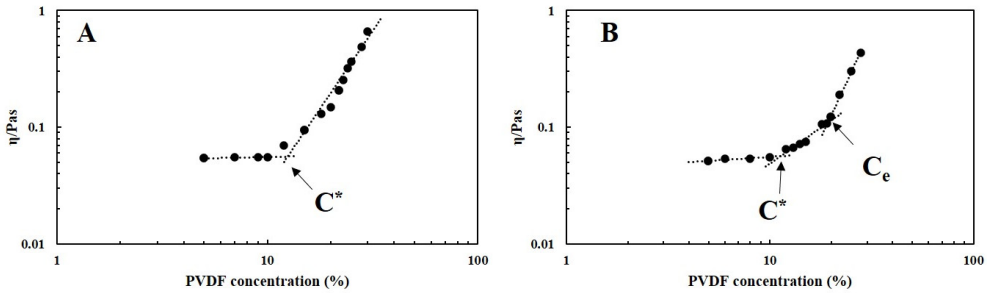

Figure 1. Viscosity (Pa·s) of the polymer solutions (**A**) PVDF in DMF, (**B**) PVDF in DMF/acetone—2/3) vs. PVDF concentration (w/v%) (circles correspond to experimental points).

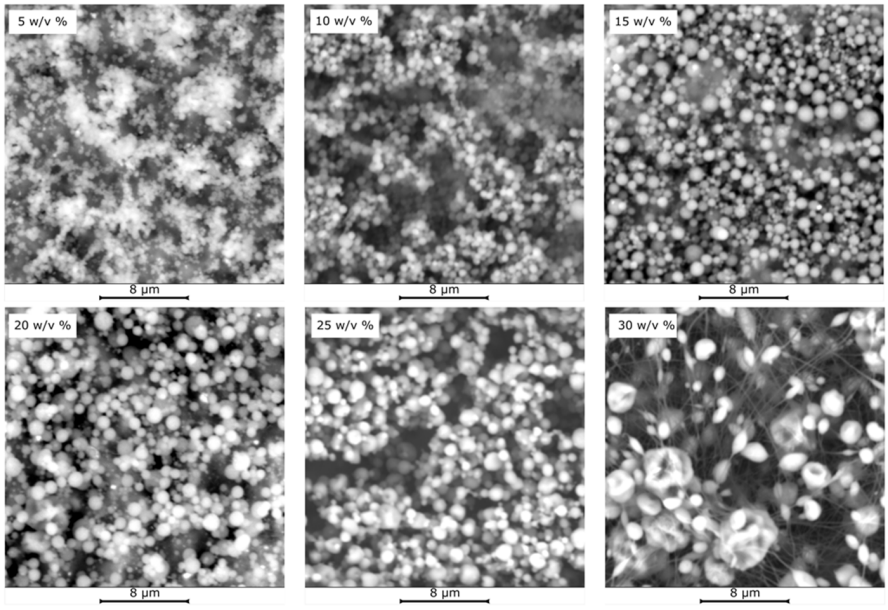

Figure 2. SEM micrographs of the electroatomized PVDF-DMF solutions (V = 20 kV, TCD = 25 cm, FR = 1 mL/h).

The use of acetone in DMF solution results in a decrease in viscosity (Figure 1B). The slope of the curve changes when the PVDF concentration is 10 *w*/*v*%, and 20 *w*/*v*%, which shows the C* of PVDF solution in the PVDF/DMF/acetone system is 10 *w*/*v*%, and the Ce of PVDF/DMF/acetone system is 20 *w*/*v*%. The structure and viscosity of electrospinning PVDF follow the rules mentioned above when most solvents can be fully volatilized. As illustrated in Figure 3, microspheres are obtained at concentrations less than 10 *w*/*v*%, and the nanofibers appear when the concentration exceeds 10 *w*/*v*%. PVDF nanofibers without beads structure can be obtained when the PVDF concentration exceeds 20 *w*/*v*% (C_e). However, when the PVDF concentration is 30 *w*/*v*%, it is difficult to continue the electrospinning process because of the jet instability and polymer deposition on the needle surface. Therefore, 25 *w*/*v*% PVDF/DMF/acetone solution was selected to discuss the factors affecting the electroactive phase of PVDF nanofibers.

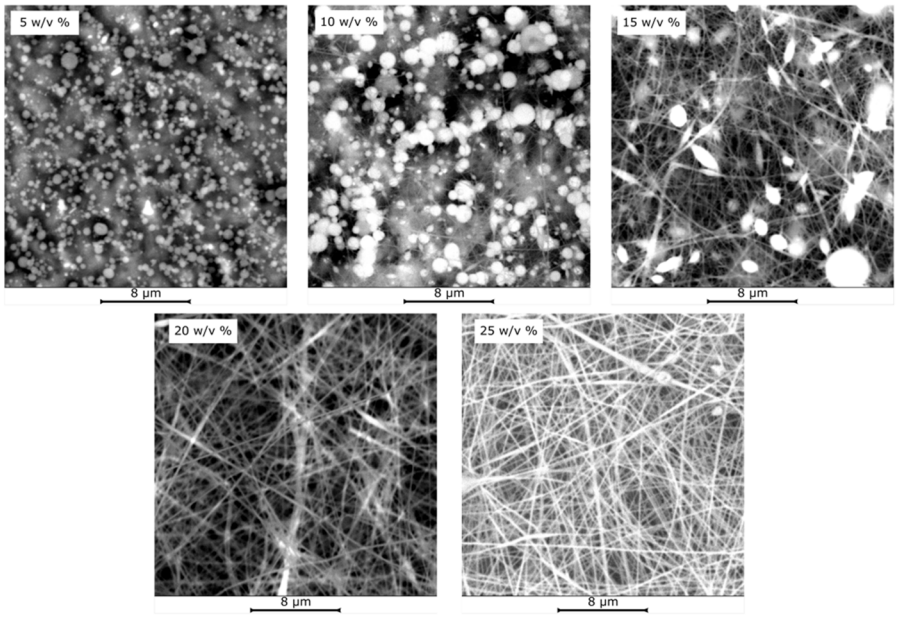

Figure 3. SEM micrographs of the electroatomized PVDF-DMF/acetone solutions (V = 20 kV, TCD = 25 cm, FR = 1 mL/h).

3.2. Factors Affecting the Electroactive Phase of PVDF Nanofibers

3.2.1. Applied Voltage

The stretching of the polymer jet under high applied voltage during the electrospinning process orients the PVDF molecular chain dipoles, allowing the α to β crystalline phase changes [42]. In the electrospinning process, applied voltage has a significant effect that can effectively stretch the polymer jet compared to other parameters (feed rate, etc.) [43]. To study the effect of stretching the polymer jet on the electroactive phase of PVDF, in this section, PVDF nanofibers obtained under different applied voltages were prepared, and the structure and properties of PVDF nanofibers and electroactive phase were discussed.

The influence of applied voltage was investigated, keeping the needle's value constant at 20 G, with a feed rate of 1 mL/h and a TCD of 20 cm. According to Figure 4A, when the voltage is 15–30 kV, the PVDF materials obtained by electrospinning are entirely nanofibers. The nanofiber diameter was recorded in Table 1. As the voltage increases, the diameter of the nanofibers decreases. This is because as the voltage increases, the increase in electric field leads to the enhanced stretching effect of Coulomb force on the jets, resulting in a decrease in the diameter of the PVDF nanofibers obtained [44]. According to Figure 4B and Table 1, as the voltage increases, the crystallinity of PVDF nanofibers does not significantly change. As the voltage increases, the stretching of the polymer jet increases, which is beneficial to the increase in crystallinity. Meanwhile, the increased electric force causes the velocity of the polymer jet to increase, resulting in a decrease in the time between the polymer solution from the needle tip to the collector, which cannot allow the macromolecular polymer chains to reorganize [45]. These two antagonistic effects cause no significant change in crystallinity as the voltage increases.

Figure 4D shows the FTIR curves of PVDF nanofibers obtained at different voltages. In these spectra, the absorbance bands at 764 cm^{-1} (CF_2 bending and skeletal bending), 795, and 975 cm^{-1} (CH_2 rocking) are due to the α phase of PVDF nanofibers [46]. An absorbance band at 840 cm^{-1} (CH_2 rocking and CF_2 stretching) is attributed to the β and γ phases [47]. The absorbance bands at 1276 and 1433 cm^{-1} (CH_2 wagging) represent the β phase [48]. The absorbance bands at 774, 812, and 1235 cm^{-1} are the existence of the γ phase [49]. The absorbance band of α, β, and γ phases do not vanish, meaning all three phases exist under different voltages. As the voltage increases, the intensity of the absorption peak at 975 cm^{-1} tends to weaken at first and then increase, showing that as the voltage increases, the α phase in PVDF nanofibers first decreases and then increases. The specific values of the electroactive phase of PVDF nanofibers prepared under different voltages can be obtained by deconvolving the peak at 840 cm^{-1} (Figure 4E). As shown in Table 1, the increase in voltage has no noticeable change on the γ phase of PVDF nanofibers, but it affects the content of β phase. With the increase in voltage, the content of electroactive phase and β phase of PVDF nanofibers increases, reaching a peak value at a voltage of 20 kV. As the voltage continues to decrease, the electroactive phase and the β phase decrease. Similar results can be obtained by deconvolving the DSC curves (Figure 4C), showing that the increase in voltage is beneficial to the production of the electroactive phase of PVDF, especially the β phase. This is due to the stretching effect of the high electric field on the polymer jet. Furthermore, this stretching effect benefits the transformation of phase α to phase β in PVDF. However, excessively high voltage causes the instability of the polymer jet and reduces the electroactive phase of PVDF, which is not conducive to the formation of the β phase.

The $F(\beta)_{Total}$ of PVDF nanofibers prepared with different voltages shows that as the voltage increases, the $F(\beta)_{Total}$ reaches the peak value at 20 kV, and as the voltage continues to increase, the $F(\beta)_{Total}$ decreases. The voltage is 20 kV, the β phase in PVDF nanofibers is the highest. The result of d_{33} shows (Table 1) that when the voltage increases from 15 to 20 kV, d_{33} increases from 9.0 to 11.4 pC/N. Increasing the voltage from 20 to 30 kV, d_{33} decreases from 11.4 to 7.8 pC/N. The PVDF nanofibers have the best piezoelectric properties when the voltage is 20 kV. The change in d_{33} is consistent with the change of

$F(\beta)_{Total}$ of PVDF nanofibers, which shows that the content of the β phase is an essential factor affecting the piezoelectric properties of PVDF.

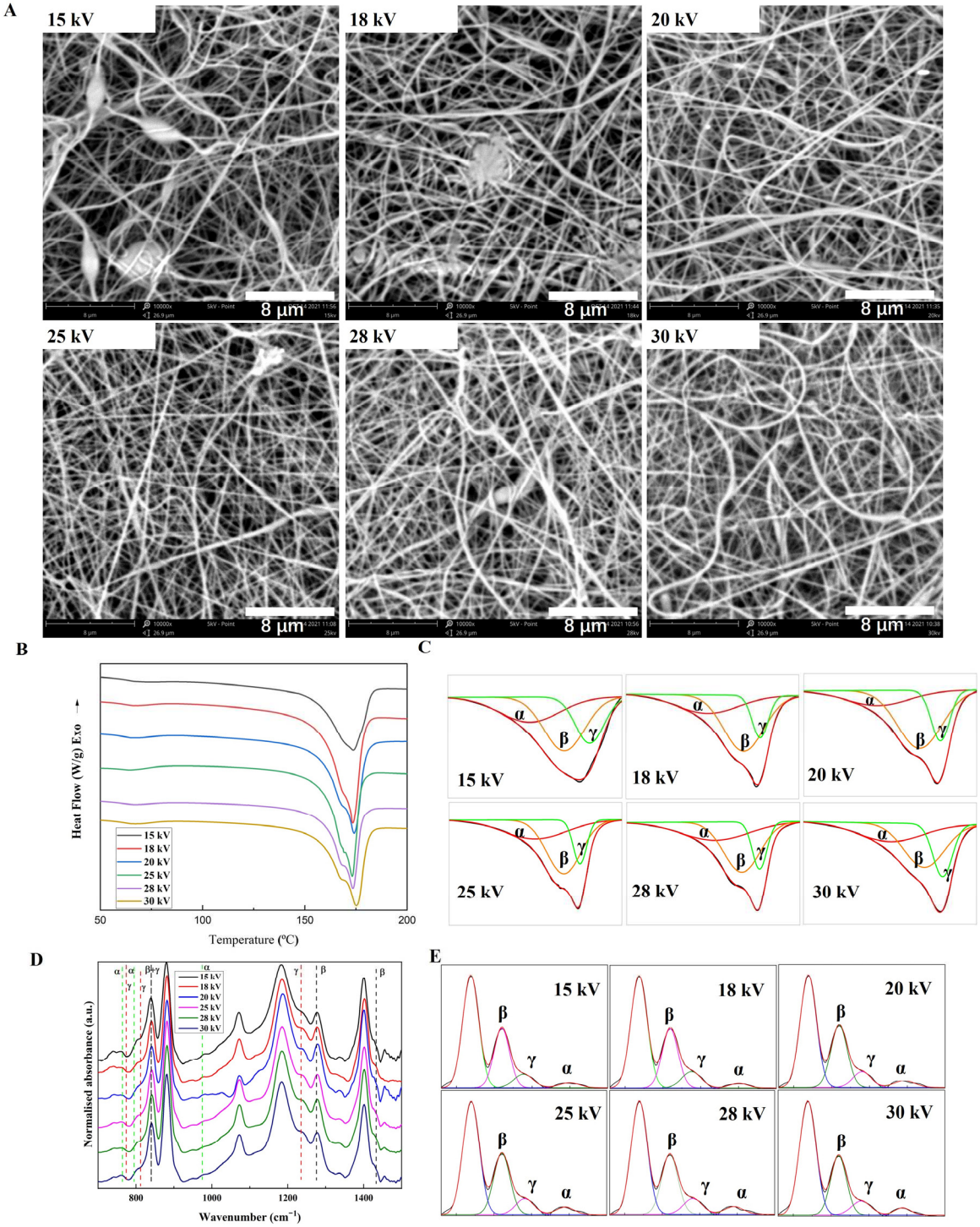

Figure 4. (**A**) SEM images, (**B**) DSC curves, (**C**) deconvolution of the DSC curves, (**D**) ATR-FTIR curves, and (**E**) deconvolution of the ATR-FTIR spectra (920–700 cm^{-1}) of PVDF nanofibers under different voltages (25 *w*/*v*% PVDF, DMF/acetone = 2/3, TCD = 20 cm, FR = 1 mL/h, V = 15–30 kV).

Table 1. The fiber diameter, F_{EA}, F(β), F(γ) and Xc data of PVDF nanofibers under different voltages (25 *w*/*v*% PVDF, DMF/acetone = 2/3, TCD = 20 cm, FR = 1 mL/h, V = 15–30 kV).

Applied Voltage (kV)		15	18	20	25	28	30
Fiber diameter (nm)		304 ± 29	296 ± 42	253 ± 44	241 ± 40	203 ± 51	190 ± 64
FTIR	F_{EA} (%)	76.5 ± 1.1	81.5 ± 1.6	92.2 ± 0.3	88.2 ± 0.5	90.6 ± 0.4	85.9 ± 1.0
	F(β) (%)	48.7 ± 1.3	55.0 ± 1.2	72.2 ± 2.1	61.7 ± 0.6	64.0 ± 0.5	58.8 ± 1.8
	F(γ) (%)	27.8 ± 0.2	26.5 ± 0.5	19.9 ± 2.0	26.5 ± 0.3	26.5 ± 0.4	27.1 ± 0.9
DSC	F_{EA} (%)	70.0	71.7	78.4	66.6	66.7	69.1
	F(β) (%)	43.6	55.0	57.6	50.4	48.4	43.9
	F(γ) (%)	26.4	16.7	20.8	16.2	18.3	25.2
	Xc (%)	36.5	48.4	45.3	43.9	41.7	38.1
	$F(\beta)_{Total}$ (%)	15.9	26.6	26.1	22.1	20.2	16.7
d_{33} (pC/N)		9.0 ± 1.3	10.8 ± 1.1	11.4 ± 2.1	8.5 ± 1.3	9.3 ± 1.0	7.8 ± 1.0
α		0.227	0.412	0.467	0.326	0.153	0.214
Goodness		0.190	0.280	0.320	0.160	0.200	0.290

3.2.2. Tip to Collector Distance (TCD)

Figure 5 shows the PVDF nanofiber structure, and the electroactive phase obtained by changing the TCD in the electrospinning process. SEM images show that with the increase in TCD from 13 to 25 cm, the structure of the beads in PVDF nanofibers decreases, and the diameter of PVDF nanofibers first increases from 254.89 to 280.34 nm and then decreases from 280.34 to 167.54 nm. The electroactive phase of PVDF nanofibers increases with the increase in TCD and reaches a peak at 25 cm (94.5% ± 0.6%). According to research, the increase in TCD is similar to the decrease in electric field intensity [50]. As the electric field intensity decreases, the stretching effect of Coulomb force on the jets is weakened, resulting in a decrease in the electroactive phase and an increase in the diameter of the PVDF nanofibers. However, the change in TCD is not consistent with this. As the TCD increases from 13 to 25 cm, the electroactive phase in PVDF nanofibers increases. This is because during the electrospinning process, the factors that affect the electroactive phase and nanofiber structure are not only the stretching effect of the electric field on the polymer jet, but also the volatilization of the solvent.

The solvents' volatility significantly affects the electrospinning result for the electrospinning PVDF solution prepared with two solvents (DMF and DMF/acetone). Incomplete solvent volatilization makes it challenging to obtain PVDF nanofibers without bead structure and adversely affects the electroactive phase of PVDF nanofibers. Incomplete solvent volatilization results in more structured beads. Compared with the fiber structure, the polymer molecular chains in the structure of the beads are difficult to polarize, which is not conducive to generating electroactive phases [44].

With the increase in TCD, on the one hand, the decrease in the electric field intensity leads to the weakening of the stretching effect of the electric field on the polymer jet. On the other hand, the solvent in the polymer solution has sufficient time to volatilize, and the electric field force fully stretches the polymer jet. Stretching reduces the formation of the beads structure, which is conducive to forming more electroactive phases. Therefore, as TCD increases, the electroactive phase in PVDF nanofibers increases.

3.2.3. Feed Rate

The feed rate is another factor that affects the stretching of the polymer jet. Figure 6 shows different electrospinning PVDF nanofibers obtained by changing the feed rate (0.3–3 mL/h) at the same voltage. The structure of PVDF nanofibers is shown in Figure 6A. The SEM images show significant beads structure at low (0.3 mL/h) and high (3 mL/h) feed rates. Additionally, with the increase in feed rate, the fiber diameter shows a trend of increasing (Figure 6B). By comparing the electroactive phases of PVDF nanofibers obtained with different feed rates (Figure 6C), it is found that as the feed rate increases,

the electroactive phase, especially the β phase, shows a trend of first increasing and then decreasing. This is because under the same voltage, as the feed rate increases, the stretching effect of the electric field on the polymer jet decreases [51]. When the feed rate is minimal (0.3 mL/h), similar to the use of too high a voltage for electrospinning, the excessive stretching of the polymer jet by the electric field leads to the instability of the polymer jet. Although the nanofiber diameter is reduced, it is not conducive to forming the electroactive phase (F_{EA} = 68.3 ± 1.2%). As the feed rate increases, the flow of the polymer jet tends to be stable, which leads to an increase in the electroactive phase. When the electroactive phase of PVDF reaches the peak value (1 mL/h, 92.4% ± 0.8%), further increasing the feed rate causes the electroactive phase to decrease because the flow of the polymer jet has stabilized; continuing to increase the feed rate only weakens the stretching effect of the electric field on the polymer jet, which eventually leads to a decrease in the electroactive phase.

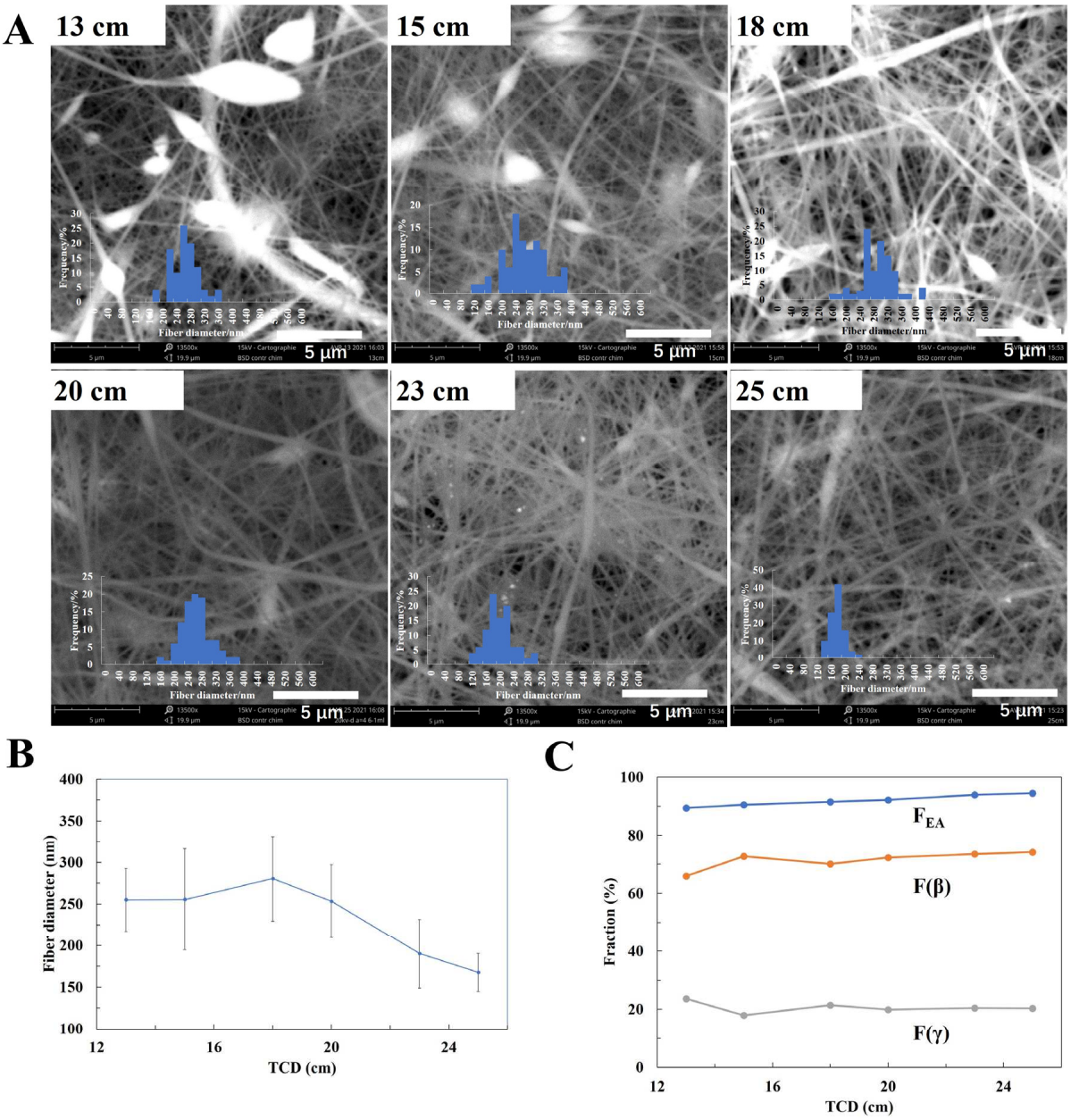

Figure 5. (**A**) SEM images and nanofibers diameter distribution, (**B**) mean nanofiber diameter, and (**C**) F_{EA}, F(β) and F(γ) of PVDF nanofibers for different TCD values (25 *w*/*v*% PVDF, DMF/acetone = 2/3, TCD = 13–25 cm, FR = 1 mL/h, V = 20 kV).

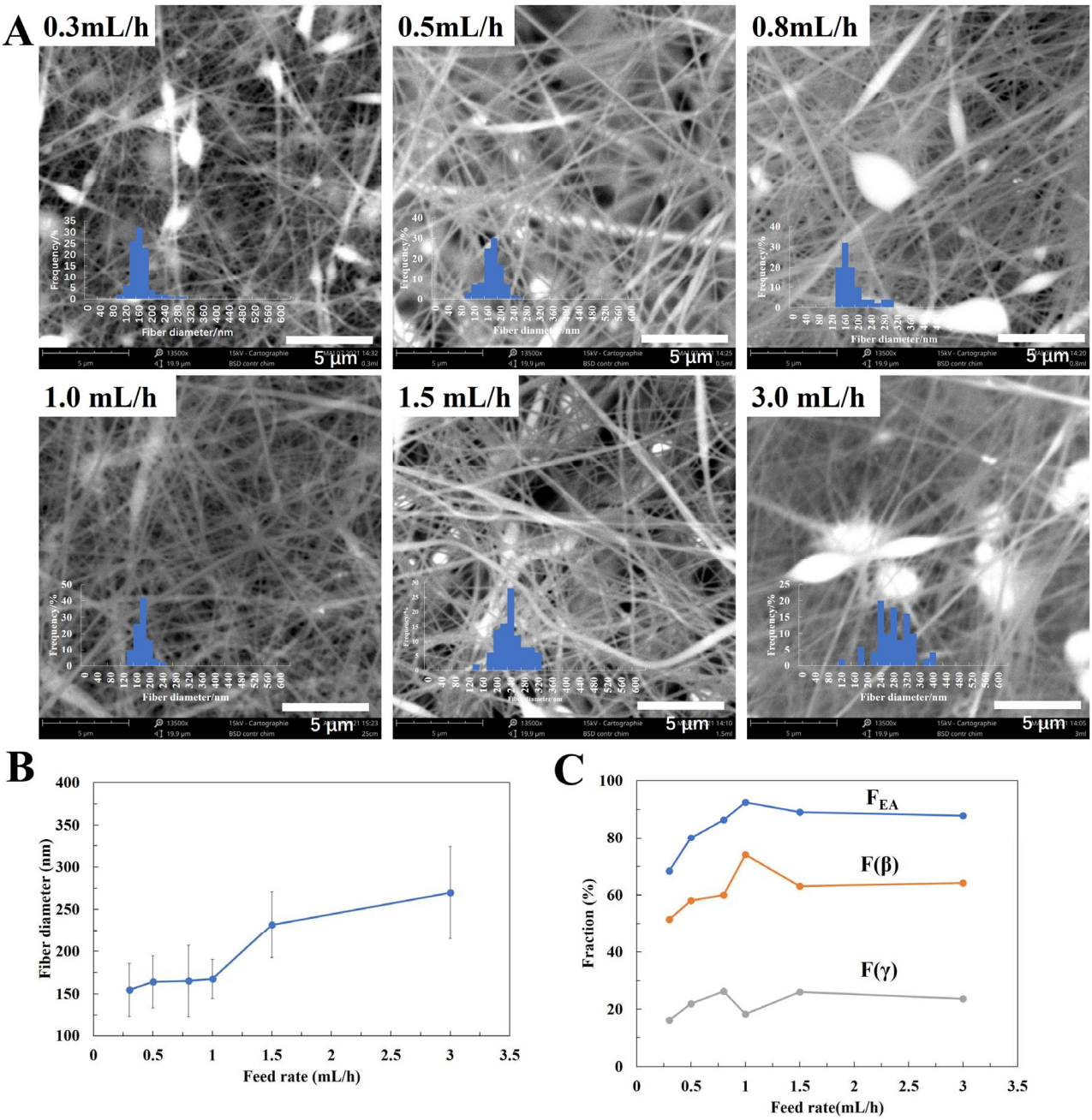

Figure 6. (**A**) SEM images and nanofibers diameter distribution, (**B**) mean nanofiber diameter, and (**C**) F_{EA}, F(β) and F(γ) of PVDF nanofibers for different FR values (25 *w*/*v*% PVDF, DMF/acetone = 2/3, TCD = 25 cm, FR = 0.3–3 mL/h, V = 20 kV).

3.2.4. Collector

In electrospinning, electric field stretching and solvent volatilization affect the polymer solution from the needle tip to a collector. Therefore, the electrospinning result can be controlled by adjusting various parameters (e.g., voltage, feed rate, and TCD). In addition, the further stretching of nanofibers is also an effective method to increase the electroactive phase. Using a mechanical stretching force to stretch the nanofibers can provide elongation forces during electrospinning and organize the lamellae to form fibers aligned along the fiber axis [52]. These facilitate the conversion of the α phase to the β phase. In this research, a rotating collector was used to stretch PVDF nanofibers mechanically, and the results are shown in Figure 6 and Table 2.

Table 2. The morphologies, thermal properties, orientation, and piezoelectric properties of PVDF nanofibers under for different rotating speeds (C) (25 *w*/*v*% PVDF, DMF/acetone = 2/3, TCD = 25 cm, FR = 1 mL/h, V = 20 kV, rotating speed: 0–2000 rpm).

Rotating Speed (Rpm)		0	200	500	1000	1500	2000
Fiber diameter (nm)		198 ± 25	191 ± 23	165 ± 50	159 ± 39	155 ± 37	134 ± 42
FTIR	F_{EA} (%)	86.7 ± 1.0	90.6 ± 1.1	87.7 ± 1.0	86.8 ± 1.1	87.4 ± 0.3	84.7 ± 1.0
	F(β) (%)	59.6 ± 2.1	63.1 ± 0.6	61.2 ± 1.4	58.0 ± 1.1	57.2 ± 3.1	55.2 ± 2.9
	F(γ) (%)	27.1 ± 0.1	27.5 ± 0.9	26.5 ± 1.6	28.8 ± 4.5	30.2 ± 4.5	29.5 ± 3.0
DSC	F_{EA} (%)	71.4	74.7	62.2	57.5	52.9	59.5
	F(β) (%)	47.5	50.2	41.8	37.9	32.5	43.1
	F(γ) (%)	23.9	24.5	20.4	19.6	20.4	16.4
	Xc (%)	42.2	44.8	41.1	41.2	36.9	42.8
	$F(\beta)_{Total}$ (%)	20.0	22.5	17.2	15.6	11.9	18.4
d_{33} (pC/N)		10.1 ± 0.8	10.7 ± 1.9	9.1 ± 1.3	8.3 ± 1.1	7.7 ± 0.7	7.2 ± 1.4
α		0.571	0.756	0.848	0.902	0.967	0.981
Goodness		0.08	0.16	0.69	0.74	0.73	0.74

The results in Figure 7 and Table 2 show that as the rotating speed increases from 0 rpm to 2000 rpm, the diameter of PVDF nanofibers decreases from 198 nm to 134 nm, and the nanofiber distribution changes from random to aligned. At the same time, as the rotating speed increases from 0 to 200 rpm, the electroactive phase of PVDF nanofibers increases from 86.7% ± 1.0% to 90.6% ± 1.1%. This is due to the mechanical stretching of PVDF nanofibers provided by the rotating collector, which enhances the orientation of the nanofibers and promotes the formation of the β phase. However, as the rotating speed increased from 500 to 2000 rpm, the electroactive phase of PVDF nanofibers decreased slightly, from 87.7% ± 1.0% to 84.7% ± 1.0%. This is because too high a rotating speed does not allow the nanofibers to be fully stretched; the nanofibers break, weakening the stretching effect [53]. The $F(\beta)_{Total}$ of PVDF nanofibers prepared with different rotating speeds shows that as the rotating speed increases, the $F(\beta)_{Total}$ reaches the peak value at 200 rpm, and the $F(\beta)_{Total}$ decreases when the rotating speed continues to increase from 500 to 2000 rpm. This shows that when the rotating speed is 200 rpm, the β phase in PVDF nanofibers is the highest. The result of d_{33} shows (Table 2) that when the rotating speed increases from 0 to 200 rpm, d_{33} increases from 10.1 to 10.7 pC/N. Continuing to increase the voltage from 200 to 2000 rpm results in d_{33} decreasing from 10.7 to 7.2 pC/N. The results of d_{33} indicated that β phase play an essential role in the piezoelectric performance of PVDF.

To quantitatively compare the arrangement of PVDF nanofibers with different rotating speeds, in this research, we used the anisotropy index (α) to describe the orientation of PVDF nanofibers. As the rotating speed increases from 0 to 2000 rpm, the α increases from 0.571 to 0.981, which means that as the rotating speed increases, the distribution of the nanofibers changed from random distribution to highly oriented distribution. Meanwhile, as the rotating speed increases from 0 to 2000 rpm, the Goodness increases from 0.08 to 0.74. Figure 8 shows the direction distribution of PVDF nanofibers. When the rotating speed is 0 rpm, the Goodness is 0.08, which means the direction distribution of the nanofibers does not fit the Gaussian distribution. When the rotating speed increases from 200 to 500 rpm, the Goodness increases from 0.16 to 0.74, which means that the direction distribution of the nanofiber increases as the rotating speed increases. The results of Table 2 and Figure 8 show that the increase in rotating speed can enhance the nanofibers' orientation and make the nanofibers more regular.

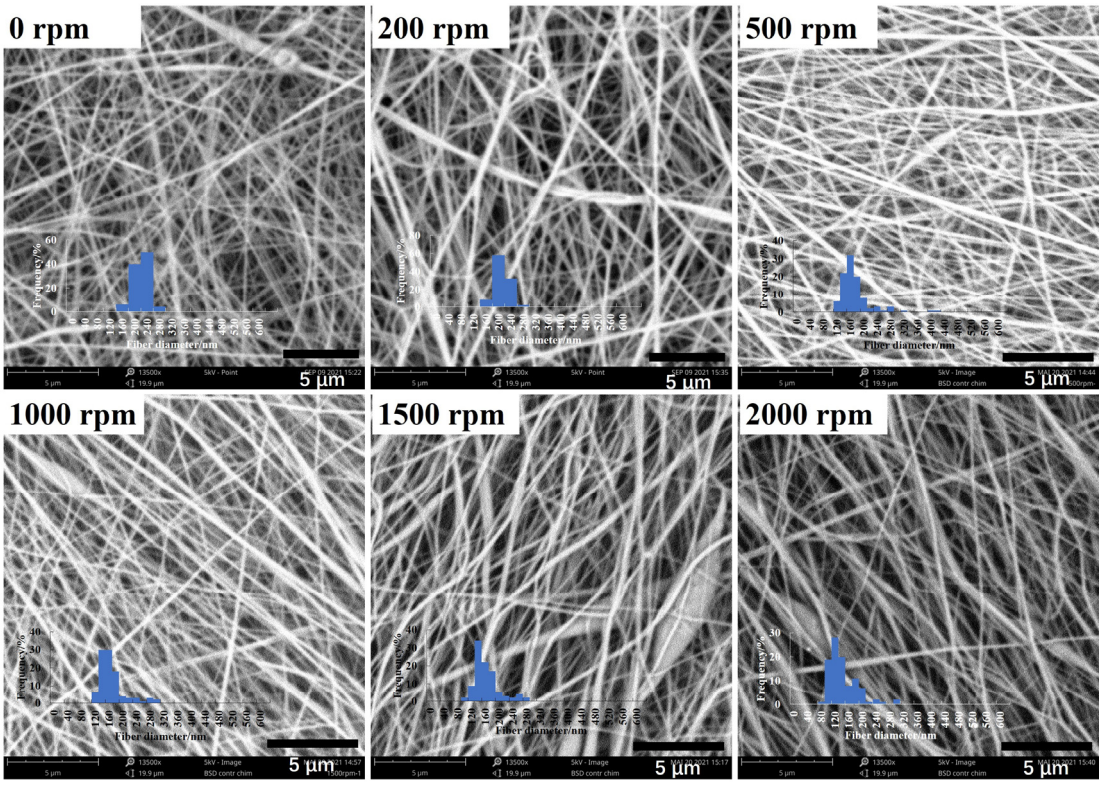

Figure 7. SEM images and nanofibers diameter distribution and nanofiber mean diameter distribution of PVDF nanofibers for different rotating speeds (C) (25 w/v% PVDF, DMF/acetone = 2/3, TCD = 25 cm, FR = 1 mL/h, V = 20 kV, rotating speed: 0–2000 rpm).

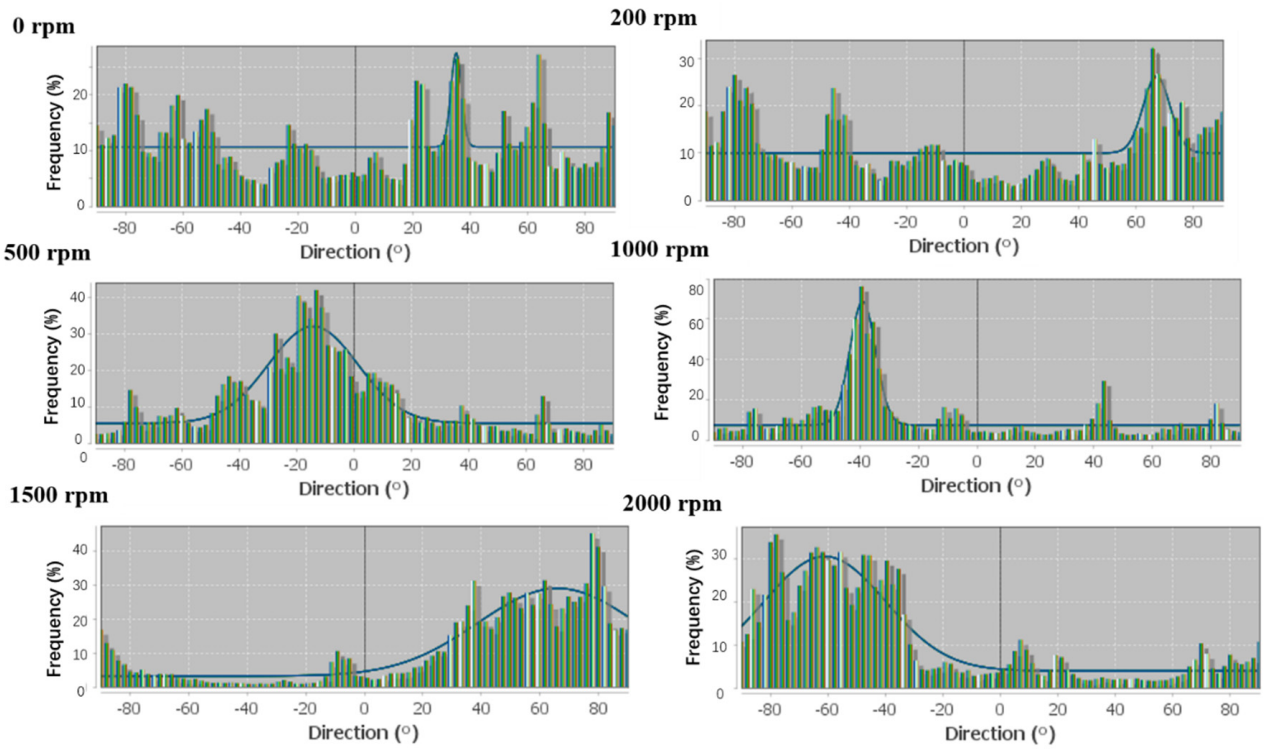

Figure 8. The orientation distribution of PVDF nanofibers for different rotating speeds (25 w/v% PVDF, DMF/acetone = 2/3, TCD = 25 cm, FR = 1 mL/h, V = 20 kV, rotating speed: 0–2000 rpm).

4. Conclusions

In this work, electrospinning PVDF nanofibers with a high electroactive phase were prepared from DMF/acetone = 2/3 (volume ratio) solutions by optimizing the PVDF concentration, voltage, feed rate, TCD, and rotating collector speed. By enhancing the stretching of the polymer jet by the electric field (increasing the voltage or reducing the feed rate), the diameter of the PVDF nanofibers can be reduced, and the electroactive phase in the PVDF nanofibers can be effectively increased. However, excessively high electric field strength causes the instability of the polymer jet, resulting in an increase in the structure of the beads and a decrease in the electroactive phase (the content of the electroactive phase decreased from 92.2% ± 0.3% to 68.3% ± 1.2%). The solvent volatilizes completely by increasing solvent volatilization (adding acetone as a mixed solvent or increasing TCD). Furthermore, fewer bead structures are generated, which can effectively improve the electroactive phase of PVDF nanofibers from 89.5% ± 0.7% to 94.5% ± 0.6%. The further stretching of PVDF nanofibers reduces the diameter of PVDF nanofibers and enhances the electroactive phase of PVDF nanofibers.

In addition, this work discussed the influence of the properties of the solution on the structure of PVDF nanofibers. The effect of four different dispersion states of polymer molecular chains in solution on electrospinning is discussed. When the solvent can be fully volatilized, PVDF nanofibers with a beadless structure can be obtained, as the concentration of the PVDF solution is greater than the entanglement concentration.

Author Contributions: Conceptualization: Z.H. and F.S.; validation: F.S., F.R. and E.M.; writing—original draft preparation: Z.H.; writing—review and editing: F.S., F.R., A.V. and E.M.; supervision, F.S., F.R. and E.M. All authors have read and agreed to the published version of the manuscript.

Funding: This work was financially supported by the GEMTEX and the China Scholarship Council (CSC).

Institutional Review Board Statement: Not applicable.

Informed Consent Statement: Not applicable.

Data Availability Statement: Not applicable.

Conflicts of Interest: The authors declare no conflict of interest.

References

1. Pathak, D.; Kumar, S.; Andotra, S.; Thomas, J.; Kaur, N.; Kumar, P.; Kumar, V. New tailored organic semiconductors thin films for optoelectronic applications star. *Eur. Phys. J. Appl. Phys.* **2021**, *95*, 10201. [CrossRef]
2. Chen, C.; Bai, Z.; Cao, Y.; Dong, M.; Jiang, K.; Zhou, Y.; Tao, Y.; Gu, S.; Xu, J.; Yin, X.; et al. Enhanced piezoelectric performance of $BiCl_3$/PVDF nanofibers-based nanogenerators. *Compos. Sci. Technol.* **2020**, *192*, 108100. [CrossRef]
3. Alhasssan, Z.A.; Burezq, Y.S.; Nair, R.; Shehata, N. Polyvinylidene difluoride piezoelectric electrospun nanofibers: Review in synthesis, fabrication, characterizations, and applications. *J. Nanomater.* **2018**, *2018*, 8164185. [CrossRef]
4. Huang, J.; Yao, M.; Yao, X. A novel approach to improving the electromechanical properties of PZT-based piezoelectric ceramics via a grain coating modification strategy. *Ceram. Int.* **2021**, *47*, 16294–16302. [CrossRef]
5. Zhang, M.; Yang, J.; Si, C.; Han, G.; Zhao, Y.; Ning, J. Research on the piezoelectric properties of AlN thin films for MEMS applications. *Micromachines* **2015**, *6*, 1236–1248. [CrossRef]
6. Shaikh, M.O.; Huang, Y.B.; Wang, C.C.; Chuang, C.H. Wearable woven triboelectric nanogenerator utilizing electrospun PVDF nanofibers for mechanical energy harvesting. *Micromachines* **2019**, *10*, 438. [CrossRef]
7. Kim, M.; Lee, S.; Kim, Y.-I. Solvent-controlled crystalline beta-phase formation in electrospun P(VDF-TrFE) fibers for enhanced piezoelectric energy harvesting. *APL Mater.* **2020**, *8*, 071109. [CrossRef]
8. Ishii, Y.; Kurihara, S.; Kitayama, R.; Sakai, H.; Nakabayashi, Y.; Nobeshima, T.; Uemura, S. High electromechanical response from bipolarly charged as-electrospun polystyrene fiber mat. *Smart Mater. Struct.* **2019**, *28*, 08LT02. [CrossRef]
9. Wang, W.; Zheng, Y.; Jin, X.; Sun, Y.; Lu, B.; Wang, H.; Fang, J.; Shao, H.; Lin, T. Unexpectedly high piezoelectricity of electrospun polyacrylonitrile nanofiber membranes. *Nano Energy* **2019**, *56*, 588–594. [CrossRef]
10. Zheng, T.; Yue, Z.; Wallace, G.G.; Du, Y.; Higgins, M.J. Nanoscale piezoelectric effect of biodegradable PLA-based composite fibers by piezoresponse force microscopy. *Nanotechnology* **2020**, *31*, 375708. [CrossRef]
11. Liu, R.Q.; Wang, X.X.; Fu, J.; Zhang, Q.Q.; Song, W.Z.; Xu, Y.; Chen, Y.Q.; Ramakrishna, S.; Long, Y.Z. Preparation of nanofibrous PVDF membrane by solution blow spinning for mechanical energy harvesting. *Nanomaterials* **2019**, *9*, 1090. [CrossRef] [PubMed]

12. Hu, X.; Jiang, Y.; Ma, Z.; He, Q.; He, Y.; Zhou, T.; Zhang, D. Highly sensitive P(VDF-TrFE)/BTO nanofiber-based pressure sensor with dense stress concentration microstructures. *ACS Appl. Polym. Mater.* **2020**, *2*, 4399–4404. [CrossRef]
13. Syu, M.H.; Guan, Y.J.; Lo, W.C.; Fuh, Y.K. Biomimetic and porous nanofiber-based hybrid sensor for multifunctional pressure sensing and human gesture identification via deep learning method. *Nano Energy* **2020**, *76*, 105029. [CrossRef]
14. Bae, J.-H.; Chang, S.-H. PVDF-based ferroelectric polymers and dielectric elastomers for sensor and actuator applications: A review. *Funct. Compos. Struct.* **2019**, *1*, 012003. [CrossRef]
15. Samadi, A.; Hosseini, S.M.; Mohseni, M. Investigation of the electromagnetic microwaves absorption and piezoelectric properties of electrospun Fe_3O_4-GO/PVDF hybrid nanocomposites. *Org. Electron.* **2018**, *59*, 149–155. [CrossRef]
16. Wan, C.; Bowen, C.R. Multiscale-structuring of polyvinylidene fluoride for energy harvesting: The impact of molecular-, micro- and macro-structure. *J. Mater. Chem. A* **2017**, *5*, 3091–3128. [CrossRef]
17. Xin, Y.; Zhu, J.; Sun, H.; Xu, Y.; Liu, T.; Qian, C. A brief review on piezoelectric PVDF nanofibers prepared by electrospinning. *Ferroelectrics* **2018**, *526*, 140–151. [CrossRef]
18. Wang, J.; Nabawy, M.R.A.; Cioncolini, A.; Revell, A.; Weigert, S. Planform geometry and excitation effects of PVDF-based vibration energy harvesters. *Energies* **2021**, *14*, 211. [CrossRef]
19. Stojanovska, E.; Ozturk, N.D.; Polat, Y.; Akbulut, H.; Kilic, A. Solution blown polymer/biowaste derived carbon particles nanofibers: An optimization study and energy storage applications. *J. Energy Storage* **2019**, *26*, 100962. [CrossRef]
20. Wang, D.; Zhang, D.; Li, P.; Yang, Z.; Mi, Q.; Yu, L. Electrospinning of flexible poly(vinyl alcohol)/MXene nanofiber-based humidity sensor self-powered by monolayer molybdenum diselenide piezoelectric nanogenerator. *Nano-Micro. Lett.* **2021**, *13*, 57. [CrossRef]
21. Singh, R.K.; Lye, S.W.; Miao, J. Measurement of impact characteristics in a string using electrospun PVDF nanofibers strain sensors. *Sens. Actuators A Phys.* **2020**, *303*, 111841. [CrossRef]
22. Khalifa, M.; Janakiraman, S.; Ghosh, S.; Venimadhav, A.; Anandhan, S. PVDF/halloysite nanocomposite-based non-wovens as gel polymer electrolyte for high safety lithium ion battery. *Polym. Compos.* **2018**, *40*, 2320–2334. [CrossRef]
23. Arumugam, R.; Srinadhu, E.S.; Subramanian, B.; Nallani, S. β-PVDF based electrospun nanofibers—A promising material for developing cardiac patches. *Med. Hypotheses* **2019**, *122*, 31–34. [CrossRef]
24. Ghosh, S.K.; Mandal, D. Synergistically enhanced piezoelectric output in highly aligned 1D polymer nanofibers integrated all-fiber nanogenerator for wearable nano-tactile sensor. *Nano Energy* **2018**, *53*, 245–257. [CrossRef]
25. Surmenev, R.A.; Chernozem, R.V.; Pariy, I.O.; Surmeneva, M.A. A review on piezo- and pyroelectric responses of flexible nano- and micropatterned polymer surfaces for biomedical sensing and energy harvesting applications. *Nano Energy* **2021**, *79*, 105442. [CrossRef]
26. Sun, J.; Zhang, Z.; Lu, B.; Mei, S.; Xu, Q.; Liu, F. Research on parametric model for polycaprolactone nanofiber produced by centrifugal spinning. *J. Braz. Soc. Mech. Sci.* **2018**, *40*, 186. [CrossRef]
27. Li, H.; Huang, H.; Meng, X.; Zeng, Y. Fabrication of helical microfibers from melt blown polymer blends. *J. Polym. Sci. Part B Polym. Phys.* **2018**, *56*, 970–977. [CrossRef]
28. He, Z.; Rault, F.; Lewandowski, M.; Mohsenzadeh, E.; Salaun, F. Electrospun PVDF nanofibers for piezoelectric applications: A review of the influence of electrospinning parameters on the β phase and crystallinity enhancement. *Polymers* **2021**, *13*, 174. [CrossRef]
29. Jiyong, H.; Yuanyuan, G.; Hele, Z.; Yinda, Z.; Xudong, Y. Effect of electrospinning parameters on piezoelectric properties of electrospun PVDF nanofibrous mats under cyclic compression. *J. Text. Inst.* **2018**, *109*, 843–850. [CrossRef]
30. Yee, W.A.; Kotaki, M.; Liu, Y.; Lu, X. Morphology, polymorphism behavior and molecular orientation of electrospun poly(vinylidene fluoride) fibers. *Polymer* **2007**, *48*, 512–521. [CrossRef]
31. Gee, S.; Johnson, B.; Smith, A.L. Optimizing electrospinning parameters for piezoelectric PVDF nanofiber membranes. *J. Memb. Sci.* **2018**, *563*, 804–812. [CrossRef]
32. Wu, C.M.; Chou, M.H.; Zeng, W.Y. Piezoelectric response of aligned electrospun polyvinylidene fluoride/carbon nanotube nanofibrous membranes. *Nanomaterials* **2018**, *8*, 420. [CrossRef]
33. Higashi, S.; Hirai, T.; Matsubara, M.; Yoshida, H.; Beniya, A. Dynamic viscosity recovery of electrospinning solution for stabilizing elongated ultrafine polymer nanofiber by TEMPO-CNF. *Sci. Rep.* **2020**, *10*, 13427. [CrossRef]
34. Barrau, S.; Ferri, A.; Da Costa, A.; Defebvin, J.; Leroy, S.; Desfeux, R.; Lefebvre, J.M. Nanoscale investigations of α- and γ-crystal phases in PVDF-based nanocomposites. *ACS Appl. Mater. Interfaces* **2018**, *10*, 13092–13099. [CrossRef]
35. Boudriaux, M.; Rault, F.; Cochrane, C.; Lemort, G.; Campagne, C.; Devaux, E.; Courtois, C. Crystalline forms of PVDF fiber filled with clay components along processing steps. *J. Appl. Polym. Sci.* **2016**, *133*. [CrossRef]
36. Cai, X.; Lei, T.; Sun, D.; Lin, L. A critical analysis of the α, β and γ phases in poly(vinylidene fluoride) using FTIR. *RSC Adv.* **2017**, *7*, 15382–15389. [CrossRef]
37. Li, Y.; Xu, M.H.; Xia, Y.S.; Wu, J.M.; Sun, X.K.; Wang, S.; Hu, G.H.; Xiong, C.X. Multilayer assembly of electrospun/electrosprayed PVDF-based nanofibers and beads with enhanced piezoelectricity and high sensitivity. *Chem. Eng. J.* **2020**, *388*, 124205. [CrossRef]
38. Shehata, N.; Elnabawy, E.; Abdelkader, M.; Hassanin, A.H.; Salah, M.; Nair, R.; Ahmad Bhat, S. Static-aligned piezoelectric poly (vinylidene fluoride) electrospun nanofibers/MWCNT composite membrane: Facile method. *Polymers* **2018**, *10*, 965. [CrossRef]
39. Qin, X.; Wu, D. Effect of different solvents on poly(caprolactone) (PCL) electrospun nonwoven membranes. *J. Therm. Anal. Calorim.* **2011**, *107*, 1007–1013. [CrossRef]

40. Tiwari, S.K.; Venkatraman, S.S. Importance of viscosity parameters in electrospinning: Of monolithic and core-shell fibers. *Mater. Sci. Eng. C* **2012**, *32*, 1037–1042. [CrossRef]
41. Gupta, P.; Elkins, C.; Long, T.E.; Wilkes, G.L. Electrospinning of linear homopolymers of poly(methyl methacrylate): Exploring relationships between fiber formation, viscosity, molecular weight and concentration in a good solvent. *Polymer* **2005**, *46*, 4799–4810. [CrossRef]
42. Kalimuldina, G.; Turdakyn, N.; Abay, I.; Medeubayev, A.; Nurpeissova, A.; Adair, D.; Bakenov, Z. A review of piezoelectric PVDF film by electrospinning and its applications. *Sensors* **2020**, *20*, 5214. [CrossRef]
43. Gheibi, A.; Bagherzadeh, R.; Merati, A.A.; Latifi, M. Electrical power generation from piezoelectric electrospun nanofibers membranes: Electrospinning parameters optimization and effect of membranes thickness on output electrical voltage. *J. Polym. Res.* **2014**, *21*, 571. [CrossRef]
44. Ribeiro, C.; Sencadas, V.; Ribelles, J.L.G.; Lanceros-Méndez, S. Influence of processing conditions on polymorphism and nanofiber morphology of electroactive poly(vinylidene fluoride) electrospun membranes. *Soft Mater.* **2010**, *8*, 274–287. [CrossRef]
45. Jiyong, H.; Yinda, Z.; Hele, Z.; Yuanyuan, G.; Xudong, Y. Mixed effect of main electrospinning parameters on the β-phase crystallinity of electrospun PVDF nanofibers. *Smart Mater Struct.* **2017**, *26*, 085019. [CrossRef]
46. Benz, M.; Euler, W.B. Determination of the crystalline phases of poly(vinylidene fluoride) under different preparation conditions using differential scanning calorimetry and infrared spectroscopy. *J. Appl. Polym. Sci.* **2003**, *89*, 1093–1100. [CrossRef]
47. Boccaccio, T.; Bottino, A.; Capannelli, G.; Piaggio, P. Characterization of PVDF membranes by vibrational spectroscopy. *J. Membr. Sci.* **2002**, *210*, 315–329. [CrossRef]
48. Li, B.; Xu, C.; Zheng, J.; Xu, C. Sensitivity of pressure sensors enhanced by doping silver nanowires. *Sensors* **2014**, *14*, 9889–9899. [CrossRef] [PubMed]
49. Liu, S.; Xue, S.; Zhang, W.; Zhai, J.; Chen, G. Significantly enhanced dielectric property in PVDF nanocomposites flexible films through a small loading of surface-hydroxylated $Ba_{0.6}Sr_{0.4}TiO_3$ nanotubes. *J. Mater. Chem. A* **2014**, *2*, 18040–18046. [CrossRef]
50. Shao, H.; Fang, J.; Wang, H.; Lin, T. Effect of electrospinning parameters and polymer concentrations on mechanical-to-electrical energy conversion of randomly-oriented electrospun poly(vinylidene fluoride) nanofiber mats. *RSC Adv.* **2015**, *5*, 14345–14350. [CrossRef]
51. Wang, S.H.; Wan, Y.; Sun, B.; Liu, L.Z.; Xu, W. Mechanical and electrical properties of electrospun PVDF/MWCNT ultrafine fibers using rotating collector. *Nanoscale Res. Lett.* **2014**, *9*, 522. [CrossRef] [PubMed]
52. Zhou, Z.; Wu, X.-F. Electrospinning superhydrophobic-superoleophilic fibrous PVDF membranes for high-efficiency water-oil separation. *Mater. Lett.* **2015**, *160*, 423–427. [CrossRef]
53. Wu, X.; Wang, Y.; Liu, J.; He, S.; Zhang, L. Improved crack growth resistance and its molecular origin of natural rubber/carbon black by nanodispersed clay. *Polym. Eng. Sci.* **2012**, *52*, 1027–1036. [CrossRef]